Supporting Information:

Stress transfer mechanisms at the sub-micron level for graphene/ polymer systems

George Anagnostopoulos[1], *Charalampos Androulidakis*[1,2], *Emmanuel N. Koukaras*[1], *Georgia Tsoukleri*[1], *Ioannis Polyzos*[1], *John Parthenios*[1], *Konstantinos Papagelis*[1,2*] and *Costas Galiotis*[1,3*]

[1]Institute of Chemical Engineering Sciences, Foundation for Research and Technology – Hellas (FORTH/ ICE-HT), P.O. Box 1414, Patras 265 04, Greece

[2]Department of Materials Science and [3]Department of Chemical Engineering, University of Patras, Patras 26504, Greece

*Whom all correspondence should be sent to: c.galiotis@iceht.forth.gr, kpapag@iceht.forth.gr

Contents:

S1 Estimate the actual laser spot size

As seen in Figure S1, the intensity of the ω_{2D} peak exhibits the characteristic s-shaped curve. The first derivative of the intensity profile is essentially a Gaussian curve and the spot size can be estimated from its FWHM to be of the order of 1.1 μm. The polarization of the incident light was kept parallel to the applied strain axis. All Raman spectra were fitted with Lorentzians curves.

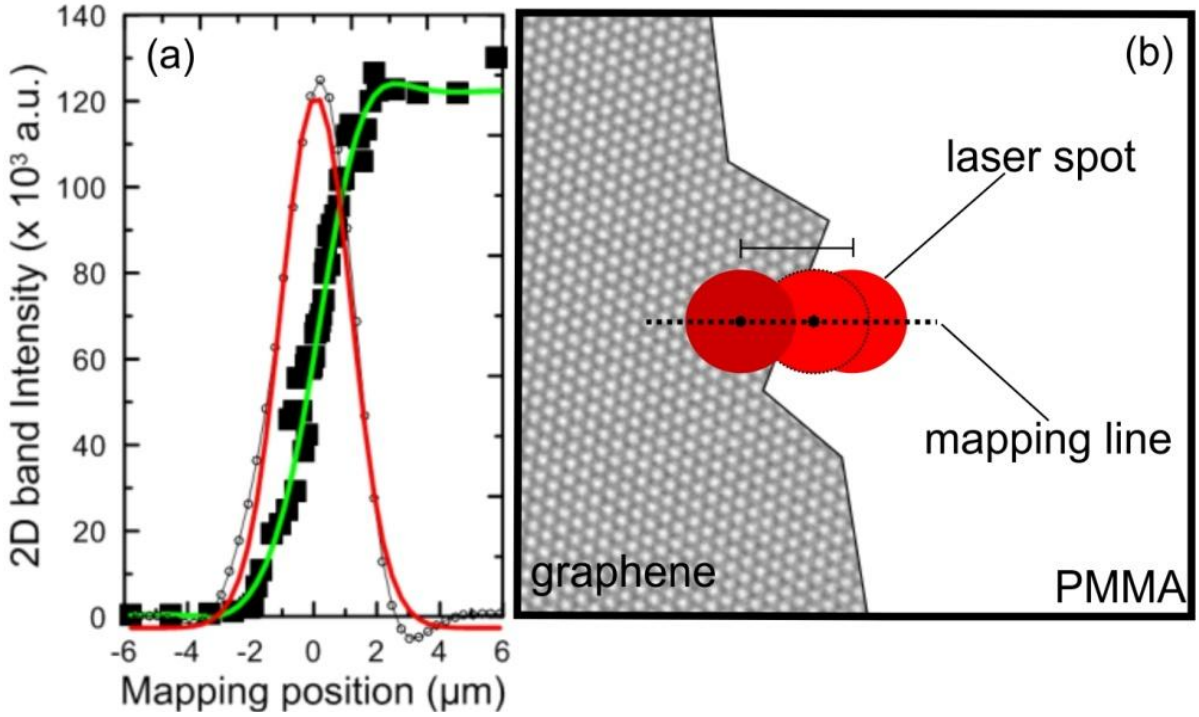

Figure S1: (a) Raman peak intensity (solid squares) as a function of the beam position across the polymer/graphene interface. The first derivative of the fitted curve (green line) provides a Gaussian profile (red line) which yields a spot size of 1.1 μm. (b). A schematic representation of the Raman mapping across the edge of a graphene flake on the SU8/PMMA system for determining the diameter of the laser beam spot.

S2. Shear field generation due to the transfer (exfoliation) process

In the following figure (Figure S2), a schematic representation of the mechanism of shear field generation that may induce compressive stressed due to the transfer (exfoliation) process is presented.

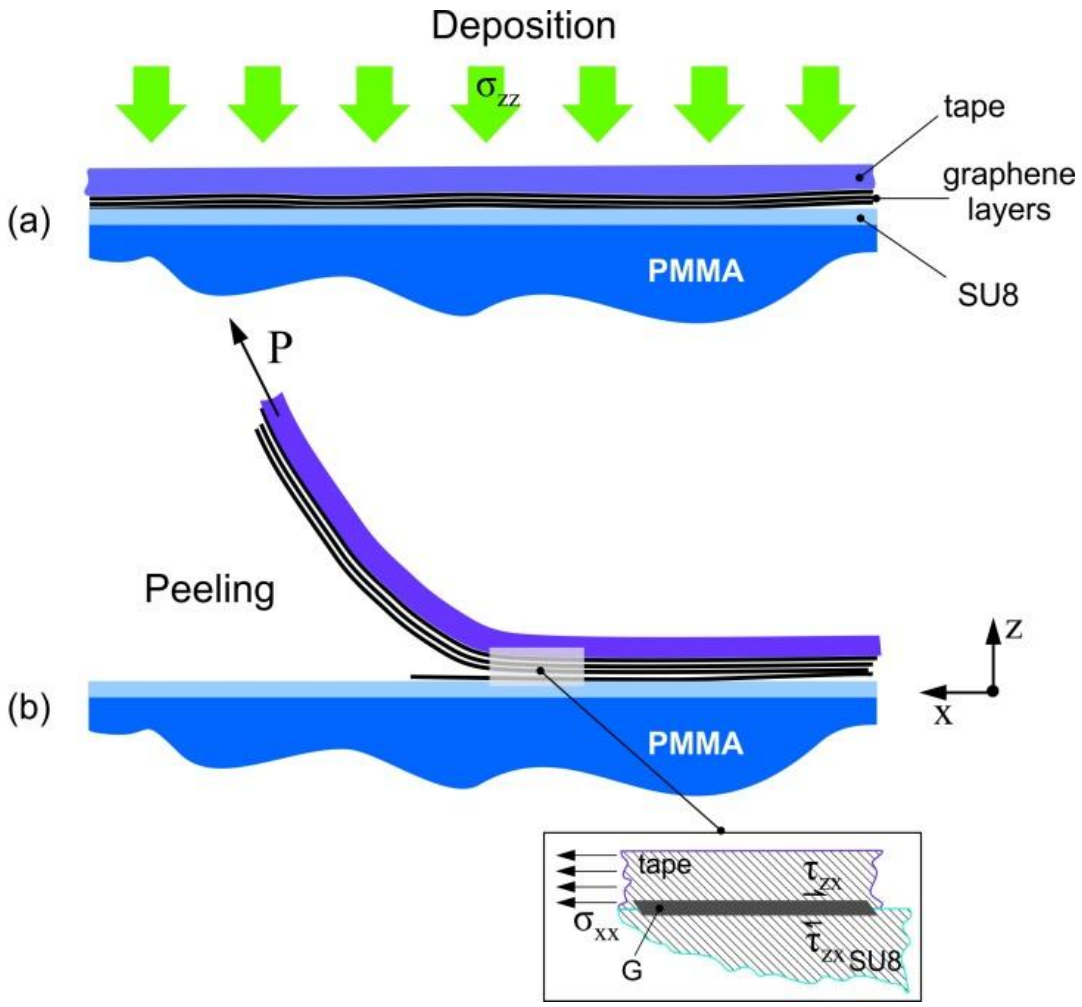

Figure S2: Schematic showing the mechanism of shear field generation due to the transfer (exfoliation) process; (a) the deposition phase under lateral pressure (thick arrows) and (b) the peeling phase. P is the peeling force and τ is the shear stress between the graphene and the tape/ graphene system and the underlying substrate. The local stresses during peeling under pressure pointing inwards (see inset) give rise to shear stresses at the interface.

S3. Presence of doping at the edges

Regarding the presence of doping, as stated elsewhere[1, 2], the as-deposited graphene appears to have excess charges due to the presence of the substrate, adsorbates and process residuals. Furthermore, according to Casiraghi et al.[3], the edges show a slightly higher doping level compares to the bulk of the flake, accompanied by a small red shift of the ω_G band and a FWHM(ω_G) decrease. In the table below is presented the average value of FWHM(ω_G) for areas close to the edges and in the bulk of the flake as an extraction from the data presented in this work.

Table S1: The average FWHM(ω_G) values at the edges and in the bulk of the graphene flake

Applied strain (%)	**FWHM (cm^{-1}) (distances: 0<x < 1500 m & 8000 < x < 9500 nm)**	**FWHM (cm^{-1}) (bulk)**
	ω_G	ω_G
0.00	11.5±1.9	13.1±1.1

S4. Indications of interface failure

An interface failure is actually depicted on the graphs below (Figure S3). A Raman mapping across the examined line was performed when the beam returned to its initial status. The distribution of ω_{2D} and ω_G with the distance show a sinusoidal form, indicating that the flake was partially delaminated from the substrate.

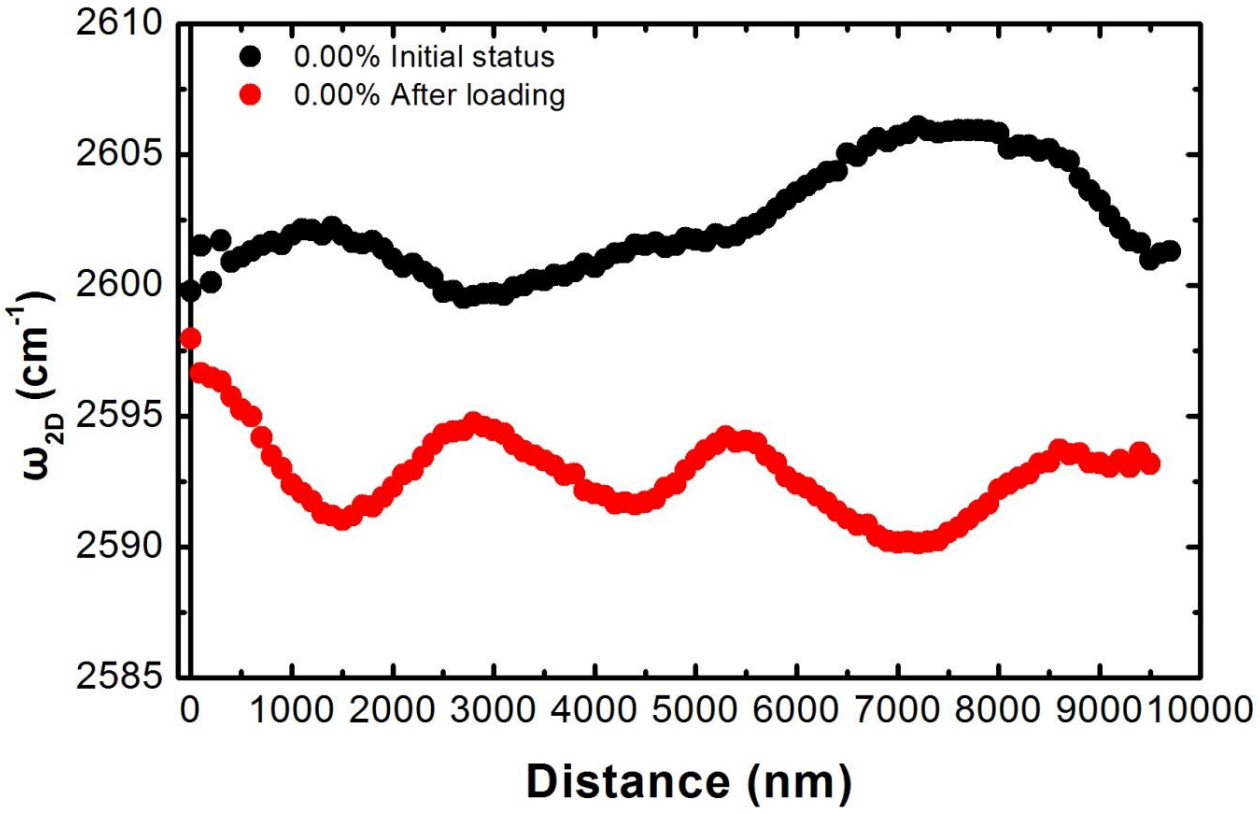

(a)

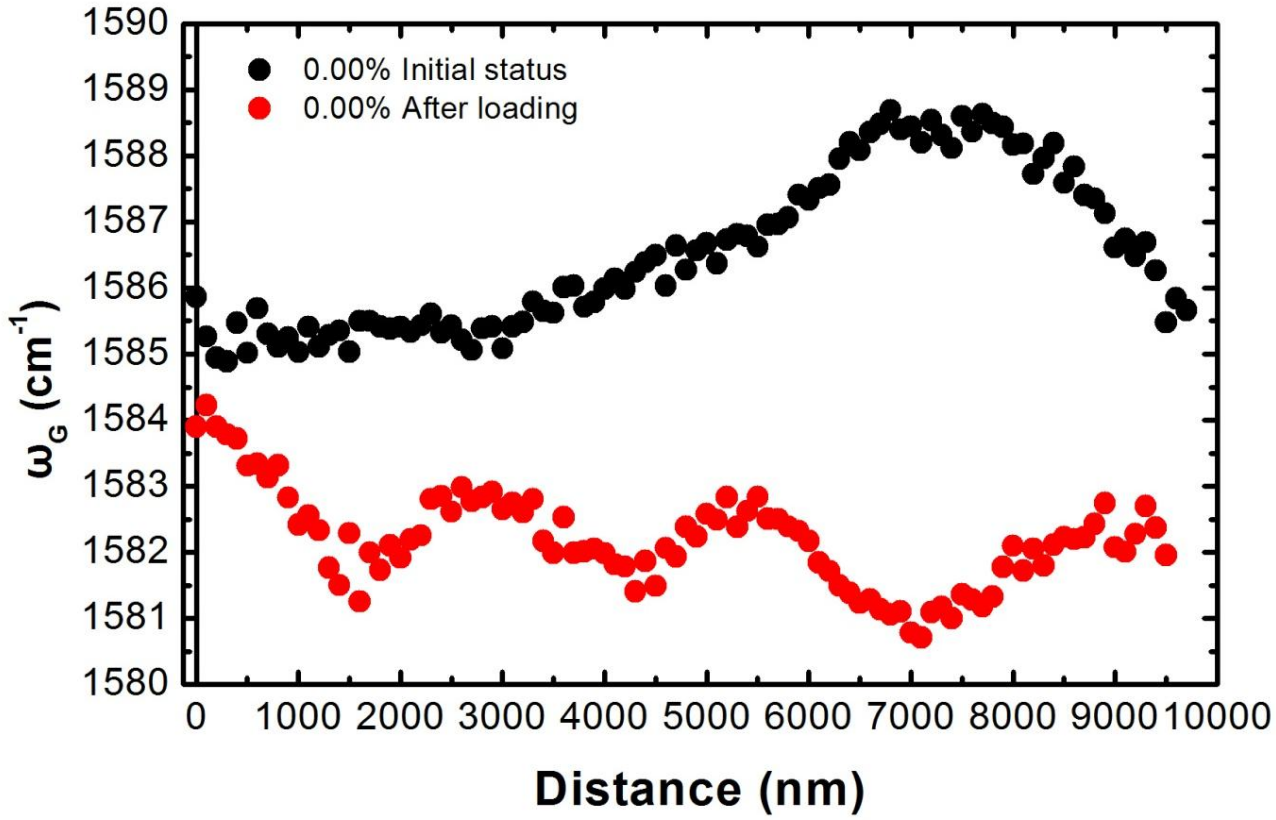

(b)

Figure S3: (a) Pos(ω_{2D}) and (b) Pos(ω_G) distributions along the mapping line before and after the application of the external load

S5. Raman wavenumber distributions of the ω_G peak for the simply supported case

To estimate the real strain applied to the graphene flake, the exact Pos(G) peak value of the graphene at 0.0% of applied strain should be known. In this case, we consider the weighted average of Pos(G) values of all the data points along the mapping line that were located within the region 3 to 5 μm as a representative ω_G value in the absence of external loading. This is found to be 1586.8 ±1.0 cm^{-1}. Then using the Pos(G) at each mapping point, the corresponding strain, ε, was estimated from the following relationship:

$$\varepsilon = \frac{(\omega_G\big|_{\varepsilon} - \omega_G\big|_{\varepsilon=0.0\%})}{k_G} \quad (1)$$

where $\omega_G\big|_{\varepsilon=0.0\%}$ = 1586.8 ±1.0 cm^{-1}, $\omega_G\big|_{\varepsilon}$ is the corresponding strain, ε, at each measured point and k_G = -19.4 cm^{-1}/% the average calibration factor of the of ω_G^- and ω_G^+ components of the ω_G Raman phonon[4].

As for the maximum ISS values, they were obtained from a suitable processing of the Raman shifts. Initially the values for the Raman shifts were converted to strain values using k_{2D} or k_G, the strain rate of the ω_{2D} or ω_G Raman band as a constant conversion factor. The datasets were then smoothed by applying a low-pass parabolic filter on their Fourier Transform (minus a baseline). The final smoothed dataset was obtained through an inverse Fourier Transform of the filtered data. The maximum ISS values then correspond (of course with the proper multiplication factors) to the points at which the first derivative of the smoothed dataset zeros out.

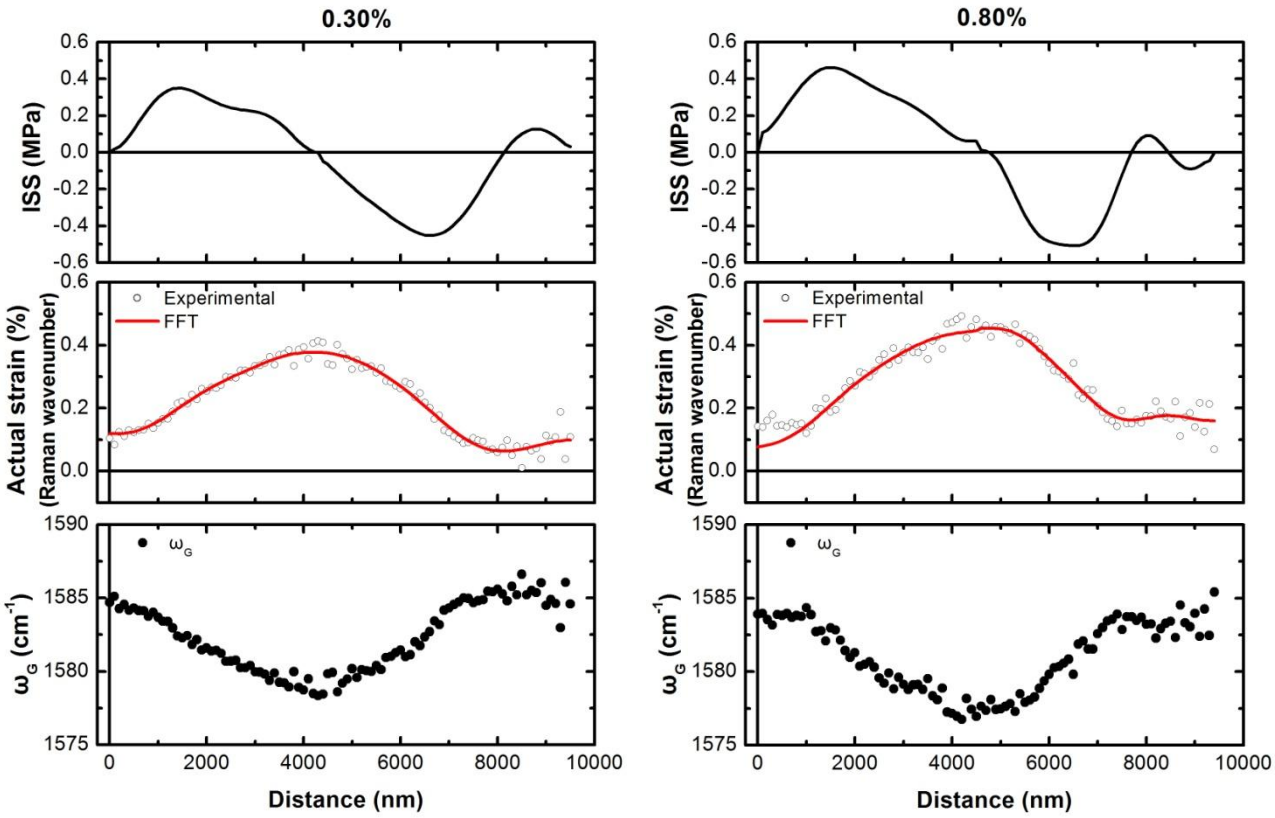

Figure S4: (lower): Raman wavenumber distributions of the ω_G peak for the simply supported case at applied strains of (a) 0.30% and (b) 0.80%. (center): The resulting axial strain distributions via the Raman wavenumber shift for (a) 0.30% and (b) 0.80%. The red solid line is a guide to the eye. (upper): The corresponding interfacial shear stress distributions along the whole length of the flake for (a) 0.30% and (b) 0.80%.

.

S6. Balance of forces on single monolayer graphene

As it is stated in our early works[5], the strain transfer profiles obtained by the Raman technique can be converted into interfacial shear stress profiles along the length of the reinforcement by means of a straightforward balance of forces argument. This indeed captures the very essence of reinforcement form a soft matrix to a stiff inclusion (eg fibre, flake etc) since the prevailing mechanism is shear at the interface which is converted into normal stress at the inclusion. Indeed, for a flake if we consider an infinitesimal flake length *dx* near its edge, then the stress equilibrium illustrated in the following figure (Figure S5) is:

$$\frac{d\sigma_x}{dx} = -\frac{\tau_t}{t_g} \Rightarrow \tau_t = -t_g \cdot E_g \cdot \frac{d\varepsilon_x}{dx} \quad (2)$$

where τ_t is the shear stress at the surface of the flake, σ_x is the axial stress of the flake and t_g is the thickness of the graphene flake [6, 7] and E_g is the graphene's Young modulus [8].

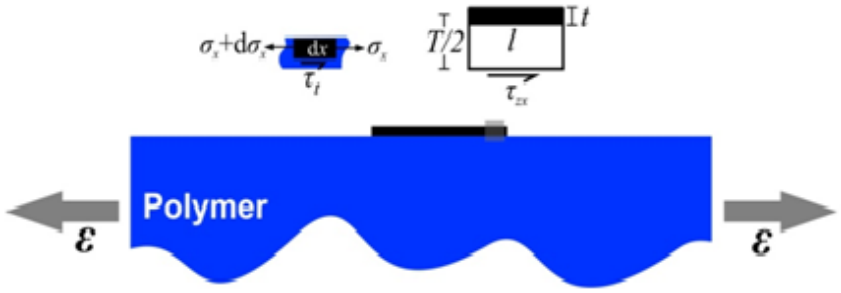

Figure S5: Illustration of stress equilibrium in a simply supported graphene flake on a polymeric bar. Axial and shear stresses in representative elements of the flake are also shown.

S7. Differences from the expected classical shear-lag distribution

A comparison between the expected Cox type strain distribution and the corresponding strain distribution of the present study is made on the following graph (Figure S6).

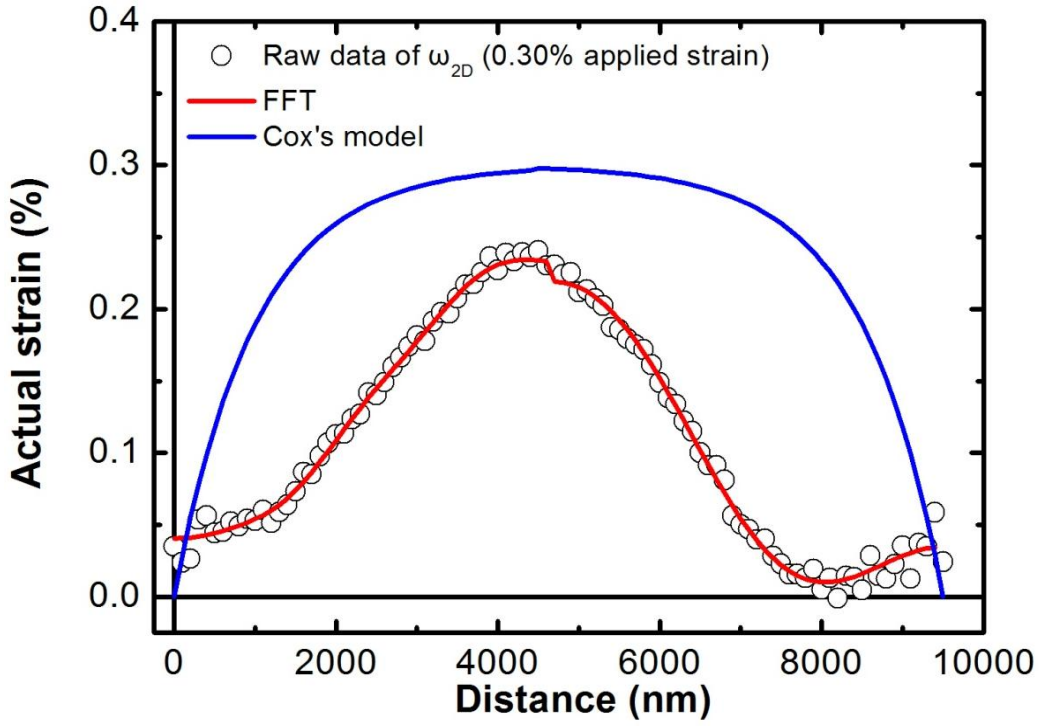

Figure S6: The axial strain distributions via Raman wavenumber shift for 0.30% of applied tensile level for ω_{2D}. The red solid line is a smoothing of the raw dataset through an inverse Fourier Transform, while the blue solid line is the application of Cox's model

Assuming that the strain rises to about 90% of the plateau value (0.30% applied strain) over about 1.5 μm from the edge of the flake[9], it seems that Cox model[10, 11] cannot follow the experimental stress distribution. The actual strain built up appeared to start at 2 μm from the edges due to the presence of doping, while for the Cox model a plateau is already reached at the corresponding distance. It is the presence of all non-mechanical interactions that take place within this distance (edge affect area), which influence the strain transfer mechanism.

S8. Simply supported case (flake 2)

A detailed Raman mapping near the edges of simply supported (Figure S7) monolayer graphene (1LG) over a SU8/ PMMA matrix by employing nanopositioning stages which allow us to make measurements at steps, as small as, 100 nm. The experimental data of the position of ω_{2D} and ω_G as a function of distance from the free end are plotted in Figure S8 for the as-received specimen but also at various increments of tensile strains up to 0.60%. As seen, systematic shifts of the ω_{2D} are obtained as one move at steps of 100 nm from the edge of the flake towards the middle and up to distance of 5 μm. These systematic shifts are evident at all strain levels but also in the as-received material. At 0.00% applied strain, there is almost a constant distribution of ω_{2D} Raman wavenumbers starting from ~2600 cm^{-1} at the edge up to a distance of 1.0 μm and then moving to lower values at greater distances.

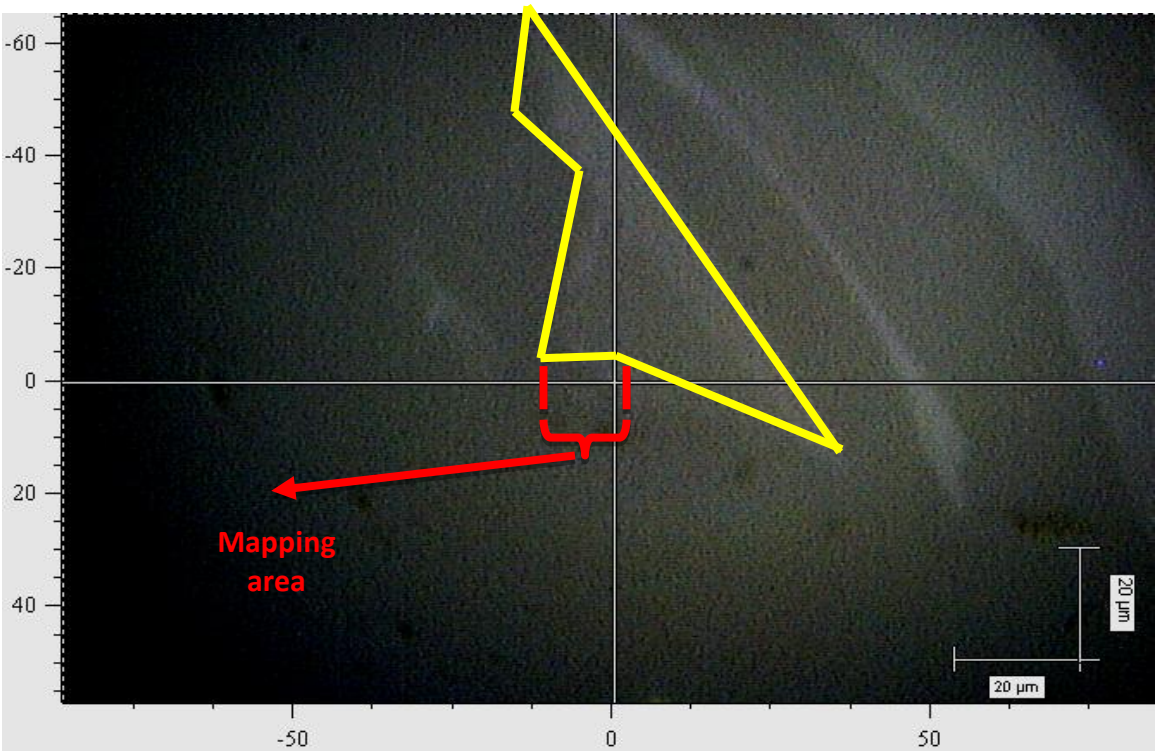

Figure S7: Optical micrograph of the simply-supported monolayer graphene (1LG)

By implementing tensile loading, there is a gradual change of slope of wavenumber over distance from positive to negative values indicating that the material is eventually subjected to tension (Figure S8). For distances greater than 1.0 μm, it seems that ω_{2D} has almost the same slope for all the applied strains (~–4.7 cm^{-1}/μm, on average), while ω_G follows a similar linear profile with almost half strain sensitivity (~–2.0 cm^{-1}/μm, on average) while their average ratio has a value of ~2.35, indicating again the dominance of the mechanical effect[12, 13].

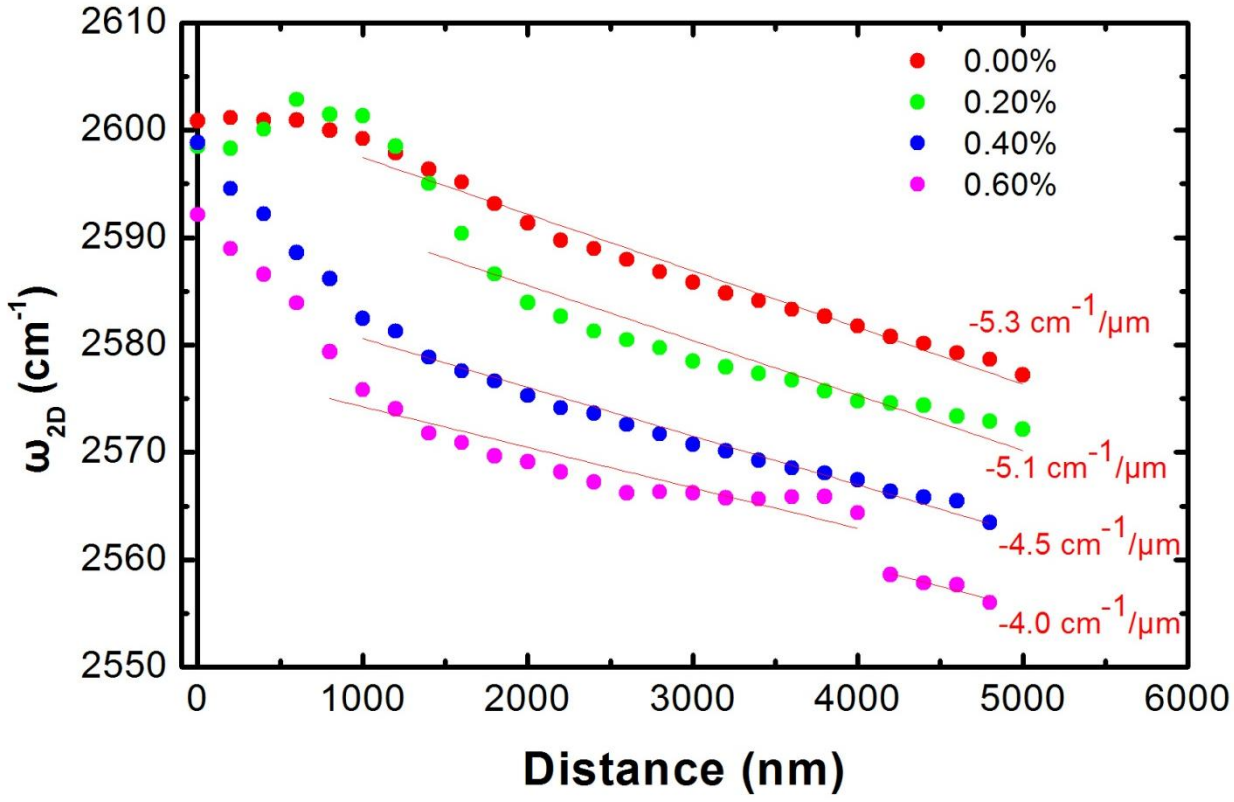

(a)

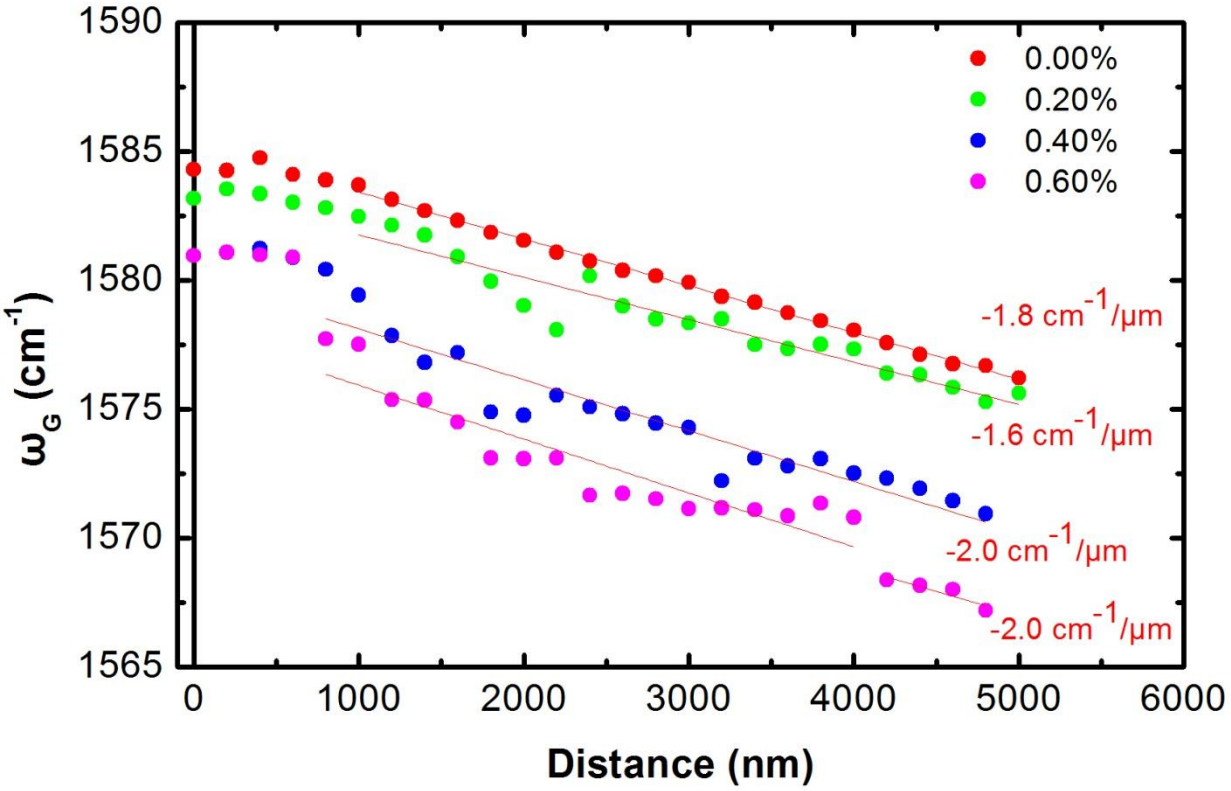

(b)

Figure S8: (a) Pos(ω_{2D}) distributions for various levels of strain are shown along a sampling line. (b) Pos(ω_G) distributions for various levels of strain are shown along a sampling line. The edge of the flake is taken as the zero distance point in order to depict the evolution of ω_{2D} and ω_G shifts with the applied strain. The measurements were taken using a 785 nm excitation laser

However, the edges are still remained in compression even at 0.60% of applied strain. It seems that up to distance of 1 μm (graphene edges), the corresponding distributions of ω_{2D} and ω_G and as result the actual strain (Figure S8) are affected by phenomena that deals either with the process production (residual stresses) or/and with the appearance of doping effects probably due to interaction of the flake with the substrate.

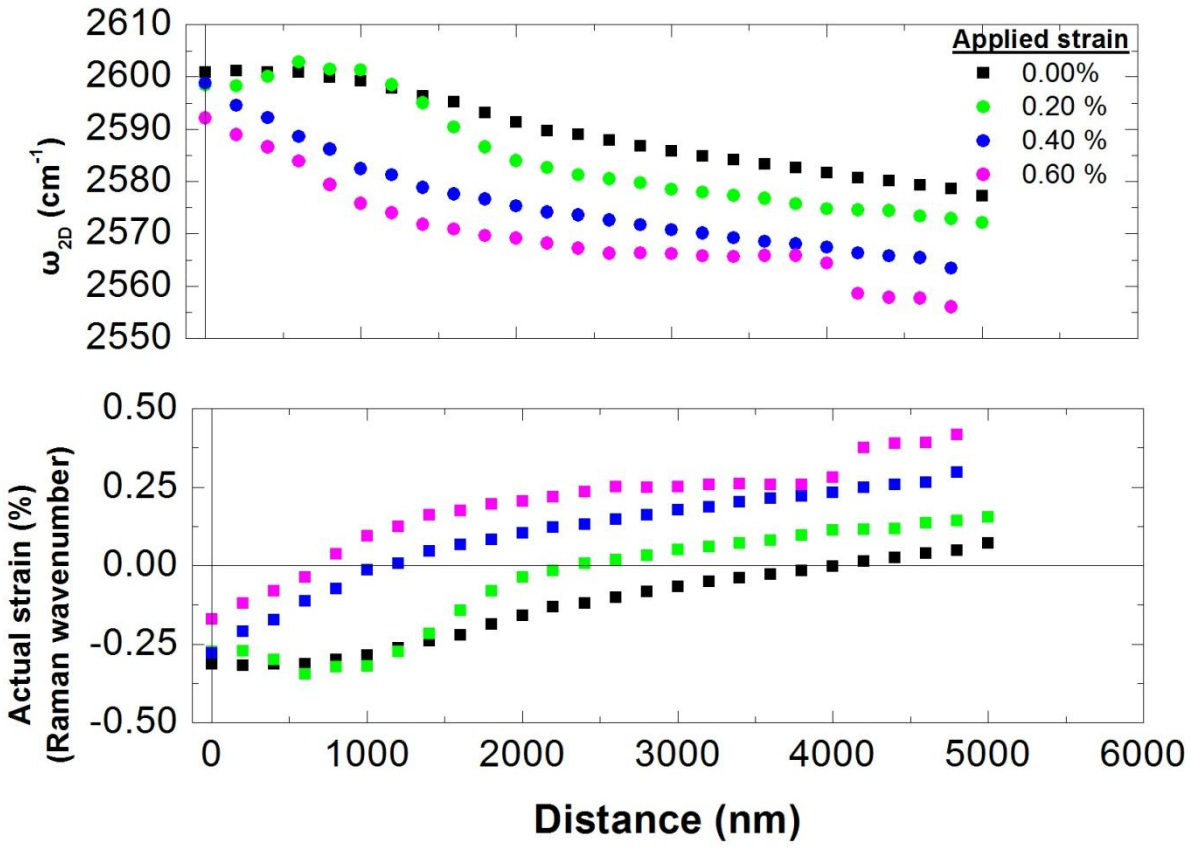

Figure S9: (upper): Raman wavenumber distributions of the Pos(ω_{2D}) for the simply supported case at all applied strains. (lower): The resulting axial strain distributions via the Raman wavenumber shift for all applied tensile strain

S9. Elastic stress transfer

As it is mentioned in the main text, the definition of the total transfer length includes the affected area due to residual stress, generated during exfoliation and deposition of the flake onto the substrate, plus the length required for elastic stress transfer. In Figure S10, an attempt is made in order to project the components of the transfer length. In Figure S10-upper and for the case of 0.30%, the area, where the external applied load is elastically transferred to the bulk of the flake, is presented. It is actually the region between the two maximum values of ISS. Within this area, the stress (strain) builds-up from the residual compressive field to the highest rate of tensile strain (Figure S10-lower).

For the 0.00% case, within the bulk of the flake, the strain field is almost zero (Figure S10-lower). However, the influences of doping species (up to 1400 nm for left hand side) and the compression field due to exfoliation procedure (at distance greater than to 6000 nm -right hand side) seems to be the main phenomena that co-exist on the flake edges (Figure S10-upper).

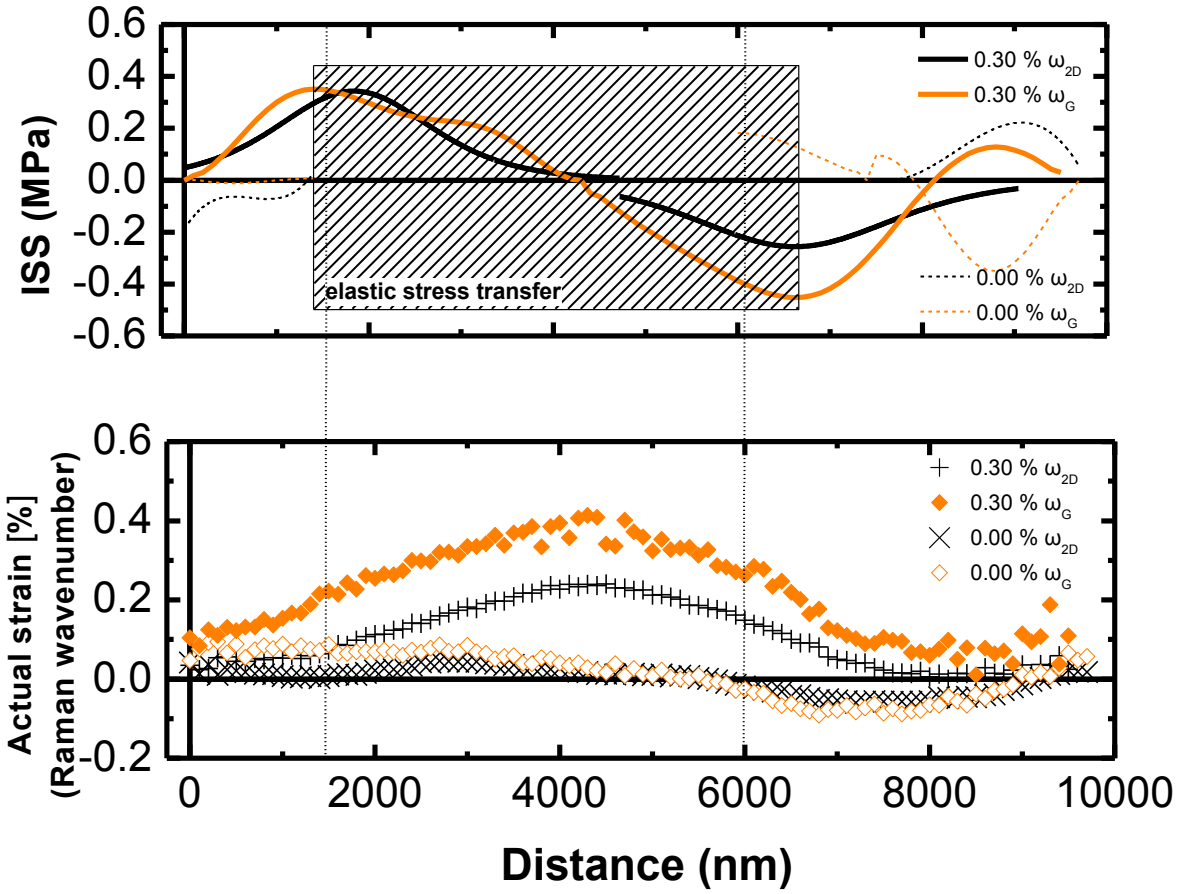

Figure S10: (upper) ISS distributions for 0.00% and 0.30% applied strain as derived by ω_{2D} and ω_G, (lower) The actual strain distribution for 0.00% and 0.30% applied strain as derived by ω_{2D} and ω_G

REFERENCES

1. Casiraghi, C. Probing Disorder and Charged Impurities in Graphene by Raman Spectroscopy. *physica status solidi (RRL) – Rapid Research Letters* 2009, 3, 175-177.

2. Casiraghi, C.; Pisana, S.; Novoselov, K. S.; Geim, A. K.; Ferrari, A. C. Raman Fingerprint of Charged Impurities in Graphene. *Applied Physics Letters* 2007, 91, 1-3.

3. Casiraghi, C.; Hartschuh, A.; Qian, H.; Piscanec, S.; Georgi, C.; Fasoli, A.; Novoselov, K. S.; Basko, D. M.; Ferrari, A. C. Raman Spectroscopy of Graphene Edges. *Nano Lett* 2009, 9, 1433-1441.

4. Frank, O.; Tsoukleri, G.; Parthenios, J.; Papagelis, K.; Riaz, I.; Jalil, R.; Novoselov, K. S.; Galiotis, C. Compression Behavior of Single-Layer Graphenes. *Acs Nano* 2010, 4, 3131-3138.

5. Galiotis, C. Interfacial Studies on Model Composites by Laser Raman Spectroscopy. *Composites Science and Technology* 1991, 42, 125-150.

6. Jeong, H.-K.; Lee, Y. P.; Lahaye, R. J. W. E.; Park, M.-H.; An, K. H.; Kim, I. J.; Yang, C.-W.; Park, C. Y.; Ruoff, R. S.; Lee, Y. H. Evidence of Graphitic Ab Stacking Order of Graphite Oxides. *Journal of the American Chemical Society* 2008, 130, 1362-1366.

7. Koh, Y. K.; Bae, M.-H.; Cahill, D. G.; Pop, E. Reliably Counting Atomic Planes of Few-Layer Graphene (N > 4). *Acs Nano* 2010, 5, 269-274.

8. Lee, C.; Wei, X.; Kysar, J. W.; Hone, J. Measurement of the Elastic Properties and Intrinsic Strength of Monolayer Graphene. *Science* 2008, 321, 385-388.

9. Gong, L.; Kinloch, I. A.; Young, R. J.; Riaz, I.; Jalil, R.; Novoselov, K. S. Interfacial Stress Transfer in a Graphene Monolayer Nanocomposite. *Adv Mater* 2010, 22, 2694-2697.

10. Cox, H. L. The Elasticity and Strength of Paper and Other Fibrous Materials. *British Journal of Applied Physics* 1952, 3, 72-79.

11. Anagnostopoulos, G.; Parthenios, J.; Andreopoulos, A. G.; Galiotis, C. An Experimental and Theoretical Study of the Stress Transfer Problem in Fibrous Composites. *Acta Materialia* 2005, 53, 4173-4183.

12. Frank, O.; Vejpravova, J.; Holy, V.; Kavan, L.; Kalbac, M. Interaction between Graphene and Copper Substrate: The Role of Lattice Orientation. *Carbon* 2014, 68, 440-451.

13. Mohiuddin, T. M. G.; Lombardo, A.; Nair, R. R.; Bonetti, A.; Savini, G.; Jalil, R.; Bonini, N.; Basko, D. M.; Galiotis, C.; Marzari, N.; Novoselov, K. S.; Geim, A. K.; Ferrari, A. C. Uniaxial Strain in Graphene by Raman Spectroscopy: G Peak Splitting, Gruneisen Parameters, and Sample Orientation. *Phys Rev B* 2009, 79.